Water Research 202 (2021) 117395

Contents lists available at ScienceDirect

Water Research

journal homepage: www.elsevier.com/locate/watres

Effect of UVC pre-irradiation on the Suwannee river Natural Organic Matter (SRNOM) photooxidant properties

Davide Palma, Amina Khaled, Mohamad Sleiman, Guillaume Voyard, Claire Richard *

Université Clermont Auvergne, CNRS, SIGMA-Clermont, ICCF, F-63000 Clermont-Ferrand, France

ARTICLE INFO

Keywords:
Natural organic matter
Carbonyls
Hydroperoxides
Chain reaction
Glyphosate
•OH radicals

ABSTRACT

The present study aimed to investigate the changes in the chemical composition, and in the optical and photooxidant properties of Suwannee River Natural Organic Matter (SRNOM) induced by UVC (254 nm) treatment. The extent of the photodegradation was first assessed by UV–visible/fluorescence spectroscopies and organic carbon analysis. An in-depth investigation of the chemical changes was also conducted using liquid chromatography-mass spectrometry and gas chromatography-mass spectrometry after derivatizations. A series of mono, di and tricarbonyls and mono and dicarboxylic acids in C_1—C_6 were identified in samples irradiated from 1 to 4 h. After 3 h of irradiation, carbonyls accounted for 46% of the organic carbon remaining in solution whereas carboxylic acids represented about 2%. Then, we investigated the modifications of the photooxidant properties of SRNOM induced by these chemical changes. At 254 nm, UVC pre-irradiated SRNOM photodegraded glyphosate 29 times faster than original SRNOM and the reaction was fully inhibited by 2-propanol (5×10^{-3} M). This enhanced photooxidant properties at 254 nm toward glyphosate was therefore reasonably due to •OH radicals formation, as confirmed by additional ESR measurements. A mechanism involving a chain reaction was proposed based on independent experiments conducted on carbonyl compounds, particularly pyruvic acid and acetone. The findings of this study show that UVC pre-treatment of NOM can enhance the removal of water pollutants and suggests a possible integration of a NOM pre-activation step in engineered water treatment sytems.

1. Introduction

Natural organic matter (NOM) is a complex mixture of organic compounds formed in soils, sediments and natural waters as a result of microbial and chemical transformation of plant tissues and microbial remains and it is an ubiquitous constituent of surface waters and drinking water supplies. NOM needs to be removed in the process of drinking water production because it can affect the color and organoleptic parameters of water and it can act as a carrier of toxic organic compounds [Zoschke et al., 2012; Tang et al., 2014]. Under UVC radiations (200–280 nm), typically used to remove bacterial and chemical contamination [Sillanpää et al., 2018], NOM undergoes extensive degradation even though complete mineralization is not usually achieved; the generation of potentially harmful by-products originating from NOM degradation is a crucial aspect of drinking water production [Buchanan et al., 2016]. Even though great efforts were put toward a better understanding of the fate of NOM in UVC treaments [Ike et al., 2019; Paul et al., 2012; Varanasi et al., 2018; S.R. Sarathy et al., 2011; Kulovaara et al., 1996; Schmitt-Kopplin et al., 1998; Corin et al., 1996; Polewski et al., 2005; Lamsal et al., 2011], many questions related to the nature of intermediary photoproducts formed and their photoreactivity remain unanswered and need to be further investigated.

Due to its heterogeneity and chemical complexity, NOM transformation was often studied by monitoring global parameters using techniques such as absorption or fluorescence spectroscopy, total organic carbon analysis, ^{13}C NMR, pyrolysis and gel permeation chromatography [Ike et al., 2019; Paul et al., 2012; Hao et al., 2020; Sarathy and Mohseni, 2007; Fukushima and Tatsumi, 2001; Schmitt-Kopplin et al., 1998; Polewski et al., 2005]. These analytical techniques allowed to assess an overall decrease of NOM UV-visible absorbance, of aromaticity and of molecular weight during oxidation processes. Several studies focused on the identification of small molecules, generated from NOM breakdown, by coupling derivatization techniques with liquid chromatography-mass spectrometry (LC-MS) or gas chromatography-mass spectrometry (GC–MS). Formation of C_1—C_4 carbonyl compounds and C_2—C_5 carboxylic acids, amino acids and

* Corresponding author.
E-mail address: claire.richard@uca.fr (C. Richard).

https://doi.org/10.1016/j.watres.2021.117395
Received 9 March 2021; Received in revised form 23 June 2021; Accepted 24 June 2021
Available online 30 June 2021
0043-1354/© 2021 The Authors. Published by Elsevier Ltd. This is an open access article under the CC BY license (http://creativecommons.org/licenses/by/4.0/).

alcohols in UVC treatments was reported [Thomson et al., 2004; Agbaba et al., 2016; Zhong et al., 2017; Corin et al., 1996]. Some of these photoproducts were also found upon irradiation of NOM with natural or simulated solar-light ($\lambda > 290$ nm) [Brinkmann et al., 2003; de Bryun et al., 2011; Goldstone et al., 2002; Kieber et al., 1990].

The presence of NOM in UVC treatments has been generally reported to lower treatment efficiency due to its ability to scavenge the reactive species generated under irradiation and/or to absorb photons competitively, therefore decreasing the degradation rate of target compounds [Wang et al., 2016]. However, NOM is able to generate oxidant species such as hydroxyl radicals (•OH), singlet oxygen ($^1O_2$) and triplet excited states (^{3}NOM*) under irradiation [Vione et al., 2014] and can also promote the degradation of contaminants during UVC treatment [Lester et al., 2013]. The photosensitizing properties of NOM may evolve during the UVC treatment because NOM itself undergoes chemical changes. Yet, to the best of our knowledge, very few studies investigated the effect of such modifications on the ability of NOM to generate photooxidants in the course of engineered water treatments. Treatments of NOM with hypochlorous acid and ozone were reported to increase its capacity to generate $^1O_2$ in simulated solar light due to the possible formation of quinone-like molecules [Mostafa and Rosario-Ortiz, 2013; Leresche et al., 2019] but also to decrease its capacity to generate ^{3}NOM* due to photosensitizers destruction [Wenk et al., 2015]. On the other hand, UV/chlorine treatment of NOM at high chlorine dosage was found to increase its ability to generate ^{3}NOM*, $^1O_2$, and •OH, upon irradiation within the range 290–400 nm [Zhou et al., 2021]. Again, these effects were proposed to be due to the formation of quinone and ketone functional groups.

The goal of this work was to study the chemical changes of SRNOM under UVC irradiation and to determine how these changes affect its photodegrading properties. In the first part, spectral changes of irradiated SRNOM solutions were monitored by UV-visible and fluorescence spectroscopies while photoproducts were analyzed by derivatization of SRNOM followed by liquid chromatography coupled to high resolution mass spectrometry (UHPLC—HRMS) or gas chromatography coupled to mass spectrometry (GC–MS). In the second part, we studied the effect of the UVC pre-irradiation on the photosensitizing properties of SRNOM. For the experiments at 254 nm, we chose glyphosate, as a probe molecule, for two reasons. It is non-absorbant at 254 nm and thus poorly subject to photolysis. Moreover, its aliphatic and saturated structure makes it difficult to oxidize except by very oxidant species such as •OH. The photooxidant properties of carbonyls at 254 nm was also studied for comparison. For the experiments at $\lambda > 300$ nm, we used recommanded probe molecules to compare the formation of •OH, ^{3}SRNOM* and singlet oxygen before and after UVC pre-irradiation [Rosario-Ortiz and Canonica, 2016].

2. Material and methods

2.1. Chemicals

SRNOM (2R101N) was purchased from the International Humic Substances Society (IHSS). Glyphosate (99.7%) and H_2O_2 (> 30%) were obtained from Fluka. Methylglyoxal (40% in weight), pyruvic acid (98%), glycolic acid (98%), acetone (> 99.5%), 2,4,6-trimethyphenol (TMP, certified reference material), furfuryl alcohol (FFA, analytical grade), terephtalic acid (98%), hydroxyl-terephtalic acid (97%), 2,4-dinitrophenylhydrazine (DNPH, 97%), bis(trimethylsilyl)trifluoroacetamide containing 1% trimethylchlorosilane (BSTFA + 1% TMCS, 98.5% exluding TMCS), NaH_2PO_4 (≥ 99.5%), Na_2HPO_4 (≥ 99%), horseradish peroxidase (52 units per mg of solid), 4-hydroxyphenylacetic acid (98%), 5,5-dimethyl-1-pyrroline-N-oxide (DMPO, > 98%) and catalase (2000–5000 units per mg of protein were purchased from and Sigma Aldrich. Water was purified by reverse osmosis RIOS 5 and Synergy, Millipore device, with resistivity 18 MΩ cm and DOC < 0.1 mg L^{-1}. All these chemicals were used as received.

2.2. UVC pre-irradiation of SRNOM

Briefly, 10 mg of SRNOM were dissolved in 250 ml of purified water to reach a concentration of 40 mg L^{-1}. SRNOM solutions were buffered at pH 7 using phosphate buffers (10^{-3} M) except for experiments conducted to monitor the pH evolution during irradiation or designed to the detection of carboxylic and hydroxylic intermediates. In these cases, SRNOM solutions were neutralized to pH = 7 ± 0.2 using freshly prepared NaOH (0.1 M). All the solutions were stored at 4 °C. SRNOM solutions (30 mL) were poured in a quartz glass cylindrical vessel (2 cm i.d. × 19 cm) and were irradiated in a device equipped with 4 germicidal tubes (253.7 nm, General Electric, 15 W). The photon flux entering the solution, corresponding to 2.9×10^{-6} Einstein.$L^{-1}.s^{-1}$, was calculated by measuring the rate of glyphosate loss in the presence of H_2O_2 (SI-Text 1, Fig SI-1). SRNOM solutions were irradiated for 1 h, 2 h, 3 h and 4 h in separate experiments and labelled $SRNOM_{1h}$, $SRNOM_{2h}$, $SRNOM_{3h}$, and $SRNOM_{4h}$, respectively. Irradiated solutions were used for analyses or sensitizing investigations within the 24 h following irradiation.

2.3. Analysis of original and UVC pre-irradiated SRNOM

UV-visible spectra were recorded on a Varian Cary 3 UV–Vis spectrophotometer. Fluorescence spectra were recorded using a Perkin Elmer LS 55 Luminescence Spectrometer. The excitation wavelength was set at 255 nm and the absorbance of solutions was adjusted at 0.10 ± 0.01 at 255 nm by dilution with purified water. The emission spectra were corrected for the dilution coefficient. Dissolved organic carbon (DOC) was measured using a Shimadzu 5050 TOC analyser. Carbonyls contained in SRNOM and irradiated SRNOM were analyzed by DNPH derivatization [Soman et al., 2008] (SI Text 2). Analyses were performed by ultra-high performance liquid chromatography (UHPLC) coupled to high resolution mass spectrometry (HRMS). HRMS was performed on an Orbitrap Q-Exactive (Thermoscientific) coupled to Ultimate 3000 RSLC (Thermoscientific) UHPLC. Analyses were run in negative (ESI^-) electrospray modes. The column was a Kinetec EVO C_{18} 100 mm / 2.1 mm, 1.7 µm (Phenomenex). Details of separation conditions are given in (SI Text 3). Molecular formulas were obtained setting the difference between experimental and accurate masses to ≤ 5 ppm while structures are proposed based on the number of DNPH molecules linked to carbonyls and on the number of double bonds in the carbonyl (NDB). In several cases, several isomers are possible and given structures are thus only indicative. Pyruvic acid and methylglyoxal were used as references to estimate the concentration of the other carbonyls (SI Text 3 and Fig. SI-2).

Carboxylic and hydroxylic intermediates were detected by a method using BSTFA derivatization (SI Text 4) followed by analysis with gas chromatography/electron impact MS (GC/EI-MS) [Yu et al., 1998]. Solutions were analyzed on an Agilent 6890 N Network gas chromatograph coupled to a 5973 Network mass selective detector and Agilent 7683B series injector. Data acquisition and processing and instrument control were performed by Agilent MSD ChemStation software. Separation conditions are described in (SI Text 4). Mass spectra were scanned between m/z 50 and m/z 500 with the source temperature set at 230 °C. Identification was based on matching query spectra to spectra present in the reference library (NIST17), with a minimum spectral similarity measure of 95%. Glycolic acid was derivatized by BSTFA as for SRNOM samples and used as a reference for the quantification of other compounds.

SRNOM and $SRNOM_{3h}$ were also analyzed by ionic Chromagraphy-Mass spectrometry (IC-MS). Details are given in SI-text 5.

2.4. Sensitizing properties of original and UVC pre-irradiated SRNOM

Glyphosate was used to probe the formation of very oxidant species such as •OH from original and pre-irradiated SRNOM solutions at 254 nm. The solutions containing glyphosate (10^{-5} M) and SRNOM were

prepared by adding 25 μL of the stock solution of glyphosate (10^{-2} M) to 10.2 mL of SRNOM (40 mg L^{-1}) and by adding purified water to reach the final volume of 25 mL. For $SRNOM_{3h}$ solutions, the same spike of glyphosate was added to 25 mL of non diluted solution. This way, the two solutions showed the same absorbance of 0.34 at 254 nm. Then, 15 mL of each solution were irradiated in the above-described device. 2-Propanol was used as a quencher of •OH. Glyphosate (10^{-5} M) was also irradiated in the presence of acetone (10^{-4} M), pyruvic acid (10^{-4} M), H_2O_2 (10^{-5} M), acetone (10^{-4} M) + H_2O_2 (10^{-5} M). Furthermore, acetone (10^{-4} M) was irradiated alone and in mixture with H_2O_2 (10^{-5} and 10^{-3} M). All these experiments were conducted in air-saturated solutions. The effect of oxygen on the rate of glyphosate photodegradation in the presence of $SRNOM_{3h}$ was studied by saturating the solution with N_2. Glyphosate concentration was monitored by UHPLC—HRMS by integrating peak area at $m/z = 168.0056$ (± 5 ppm). AMPA (aminomethylphosphonic acid) with $m/z = 110.0002$ (± 5 ppm) was the only glyphosate photoproduct detected. Acetone loss and photoproducts formation were monitored by derivatization with DNPH followed by UHPLC—HRMS analysis. Photodegrading properties of SRNOM and $SRNOM_{3h}$ solutions were also investigated under irradiation between 300 and 400 nm. Both solutions were diluted by a half during preparation of mixtures. Terephthalic acid (2×10^{-5} M) was used to probe •OH radicals, 2,4,6-trimethyphenol (2×10^{-5} M) to probe ^{3}SRNOM* and $^3SRNOM_{3h}$* and furfuryl alcohol (5.8×10^{-5} M) to trap $^1O_2$. Solutions buffered at pH 7 were irradiated in a device equipped with 6 fluorescent tubes emitting between 300 and 400 nm [Palma et al., 2020]. Pseudo-first-order rate constants of probes phototransformation were determined by plotting $\ln(C_t/C_0) = k \times t$, where C_t and C_0 are the probe concentration at time t and before irradiation. All the experiments were duplicated.

2.5. Peroxides titration

Peroxides concentration was measured by the spectrofluorimetric quantification method previously described by Miller and Kester, 1988. Details of the experiments are given in SI-text 6.

2.6. ESR experiments

ESR experiments were carried out using a Bruker EMX, 9.8 GHz equipped with a cavity ER4105DR and a xenon lamp (Xenovia 200 - 900 nm). The ESR spectra were obtained at room temperature under

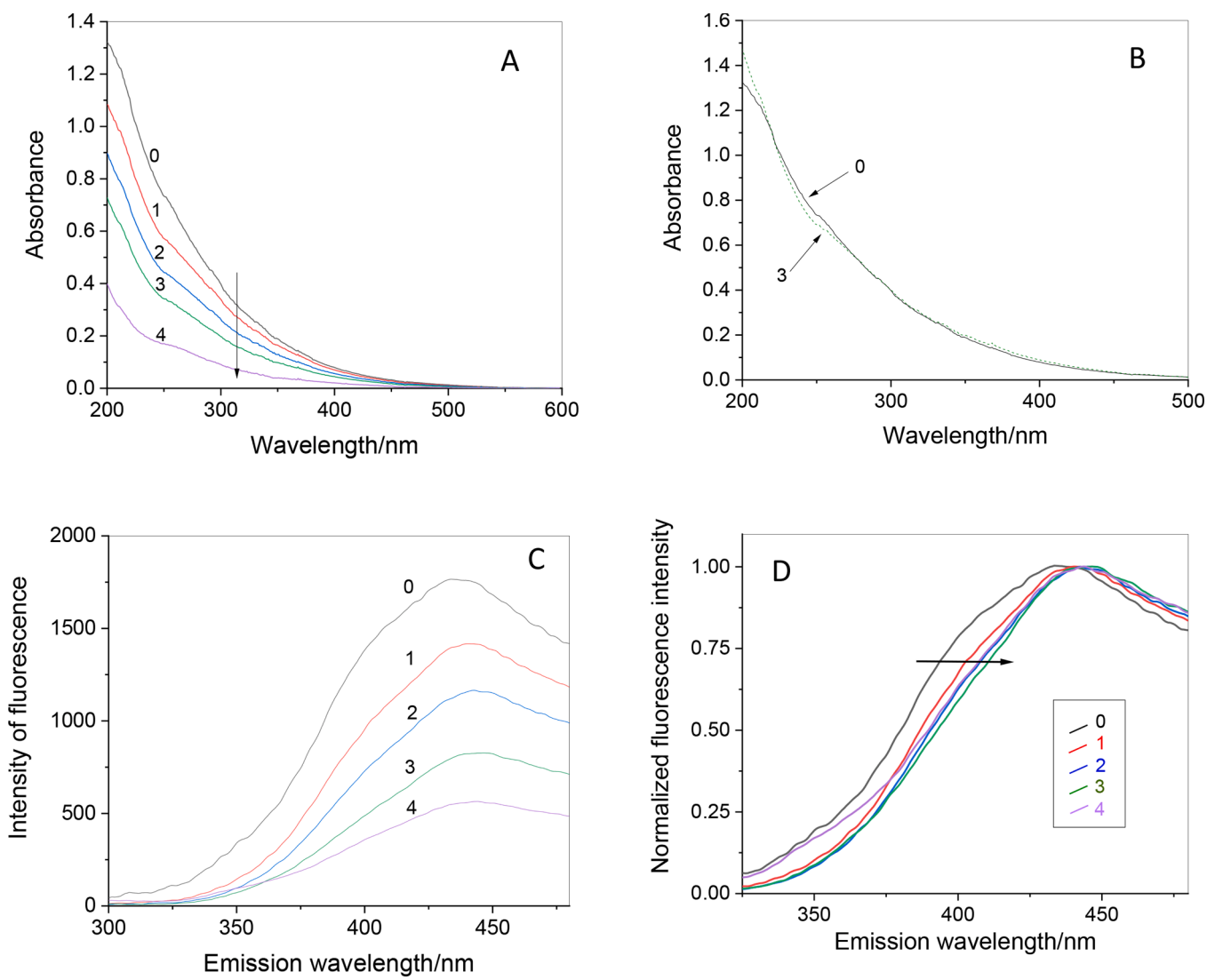

Fig. 1. Spectral changes of SRNOM solution (40 mg L^{-1}, phosphate buffers pH 7) upon irradiation at 254 nm. Curve 0: $t = 0$; curve 1: $t = 1$ h; curve 2: $t = 2$ h; curve 3: $t = 3$ h; curve 4: $t = 4$ h. A and B: UV-visible spectra. In B, curve 3 is rescaled to have the same absorbance at 300 nm as curve 0. C and D: Fluorescence spectra recorded at an excitation wavelength of 255 nm, and an absorbance adjusted at 0.10 ± 0.01 at 255 nm. In C, spectra are corrected for the dilution coefficient. In D, spectra are normalized by their respective maximum fluorescence intensity.

irradiation inside the cell of the following mixtures: DMPO (25 mM) in the presence of SRNOM (20 mg L^{-1}), $SRNOM_{3h}$ or H_2O_2 (5×10^{-3} or 10^{-5} M).

3. Results and discussion

3.1. Spectral changes of SRNOM upon 254-nm irradiation

Fig. 1A shows that the SRNOM solution progressively photobleached. The absorbance at 254 nm declined by 59% and 77% after 3 and 4 h of irradiation, respectively (Table 1). The reduction of DOC as a function of irradiation time revealed that SRNOM also underwent substantial mineralization (35% after 4 h) while the specific ultraviolet absorbance (SUVA) decreased by 42% and 64% after 3 and 4 h of irradiation, respectively, indicating a loss of unsaturated/aromatic moieties [Weisshar et al., 2003] (Table 1). Yet, the spectrum shape (Fig. 1B) and the E_2 / E_3 ratio (Table 1) did not change much indicating that photoproducts negligibly contributed to the absorption and were poorly absorbing compounds.

Irradiation also led to a breakdown of fluorescent species in accordance with previous studies [Patel-Sorrentino et al., 2004]. The fluorescence intensity at the emission maximum declined by 53% after 3 h of irradiation, and by 68% after 4 h (Fig. 1C). Fig. 1D also shows that the blue part of the fluorescence emission spectra disappeared the fastest leading to emission spectra red-shifted by 10 - 15 nm or to a band contraction. On the contrary, treatment of NOM with radicals such as $SO_4\bullet^-$ [Zhang et al., 2019] or •OH [Varanasi et al., 2018] was reported to induce a blue-shift of fluorescence emission spectra attributed to preferential degradation of high molecular weight moieties into smaller entities. In these treatments, radicals are expected to react preferentially with biggest macromolecules offering the largest number of attack sites while in photolytic treatment the reactivity of generated excited states is the critical factor. Our results suggest that smaller fluorescent entities initially present in SRNOM or produced in the course of the treatment were more subject to photodegradation than larger ones. The reasons could be that they were more light absorbing because more oxidized and/or underwent less desactivation processes than bigger constituents being less embedded in large structures than these latter.

3.2. Carbonyls and carboxylic acids formation upon 254-nm irradiation of SRNOM

Table 2 summarizes the chemicals detected by DNPH or BSTFA derivatization and by CI/MS in SRNOM before irradiation and after irradiation. Detailed MS data are given in Figure SI-3, Tables SI-1 to SI-3 and the structures of photoproducts observed in irradiated samples are shown in Fig. 2. In starting SRNOM, we detected 5 carbohydrates in C_5 and C_6 (xylose, rhamnose, fucose, glucose and galactose) mentionned in the IHSS web page, along with 2 monocarboxylated alkanes in C_3 and C_{18} (glyceric and oleic acids) and 3 dicarboxylated alkanes in C_6, C_9 and C_{12} (hexanedioic, nonanedioic and dodecanedioic acids) (Tables 2 and SI-1). Several carbonyls were found, but only as traces.

In $SRNOM_{3h}$, none of the carbohydrates observed in SRNOM were found while 11 carboxylated alkanes were detected: 5 monocarboxylated in C_1 (formic acid), C_2 (acetic and glycolic acid), C_3 (lactic acid) and C_4 (4-aminobutanoic acid), 7 dicarboxylated alkanes in C_2 (oxalic acid), C_3 (malonic, tartronic, dihydroxymalonic acids), C_4 (butanedioic and malic acids), C_5 (glutaric acid) and C_6 (tricarballylic acid) (Tables 3 and SI-2). In all the irradiated samples, 16 carbonyls in C_1—C_5 were detected among them 7 monocarbonyls (formaldehyde, acetaldehyde, glycoladehyde, glyoxylic acid), 7 dicarbonyls (glyoxal, methylglyoxal, butenedial) and 2 tricarbonyls. Some of these compounds were already reported to be produced by irradiation of natural surface waters or synthetic waters containing NOM with natural or simulated solar-light, by ozone treatment or by UV-based AOPs of solutions of humic substances. This is the case for formic, acetic and oxalic acids [Brinkmann et al., 2003; Goldstone et al., 2002], formaldehyde, acetaldehyde, glyoxal and methylglyoxal [Thomson et al., 2004; Agbaba et al., 2016; Zhong et al., 2017; de Bryun et al., 2011; Kieber et al., 1990], malonic and butanedioic acids [Corin et al., 1996], and pyruvic acid [Thomson et al., 2004].

The concentration of the different carbonyls after 1, 2, 3 and 4 h of irradiation were estimated using derivatized methylglyoxal and pyruvic acid (Table SI-4). Fig. 3A shows the concentration profile of the most concentrated ones, i.e. formaldehyde, glyoxylic acid, pyruvic acid, glyoxal and glycolaldehyde, as a function of irradiation time. The concentration of formaldehyde and glyoxylic acid was maximum after 2 h of irradiation and then declined while that of pyruvic acid, glyoxal and glycolaldehyde increased throughout the 4 h of irradiation. It shows that

Table 1
Spectral parameters of original and pre-irradiated SRNOM.

NOM	A_{254}	DOC (mg L^{-1})	SUVA (L mgC^{-1} m^{-1})	E_2/E_3
SRNOM	0.83	15.6	5.34	4.88
$SRNOM_{1h}$	0.58	13.7	4.24	3.79
$SRNOM_{2h}$	0.42	13.3	3.16	3.36
$SRNOM_{3h}$	0.34	10.9	3.12	3.69
$SRNOM_{4h}$	0.19	10.1	1.92	4.70

Table 2
Chemicals detected in SRNOM and photoproducts detected in irradiated SRNOM.

Compound	N°	Name	Method of detection	Samples in which the compound was detected
CH_2O	1	formaldehyde	DNPH	$SRNOM_{1h,2\ h,3\ h,4h}$
CH_2O_2	2	formic acid	CI/MS	$SRNOM_{3h}$
C_2H_4O	3	acetaldehyde	DNPH	$SRNOM_{1h,2\ h,3\ h,4h}$
$C_2H_4O_2$	4	acetic acid	CI/MS	$SRNOM_{3h}$
$C_2H_4O_2$	5	glycolaldehyde	DNPH	$SRNOM_{1h,2\ h,3\ h,4h}$
$C_2H_2O_2$	6	glyoxal	DNPH	$SRNOM_{1h,2\ h,3\ h,4h}$
$C_2H_4O_3$	7	glycolic acid	BSTFA	$SRNOM_{3h}$
$C_2H_2O_3$	8	glyoxylic acid	DNPH	$SRNOM_{1h,2\ h,3\ h,4h}$
$C_2H_2O_4$	9	oxalic acid	CI/MS	$SRNOM_{3h}$
$C_3H_4O_2$	10	methylglyoxal	DNPH	$SRNOM_{1h,2\ h,3\ h,4h}$
$C_3H_6O_3$	11	lactic acid	BSTFA	$SRNOM_{3h}$
$C_3H_4O_3$	12	pyruvic acid	DNPH	$SRNOM_{1h,2\ h,3\ h,4h}$
$C_3H_2O_3$	13		DNPH	$SRNOM_{1h,2\ h,3\ h,4h}$
$C_3H_2O_4$	14		DNPH	$SRNOM_{1h,2\ h,3\ h,4h}$
$C_3H_4O_4$	15	malonic acid	BSTFA	$SRNOM_{3h}$
$C_3H_6O_4$	16	glyceric acid	BSTFA	SRNOM
$C_3H_4O_5$	17	tartronic acid	BSTFA	$SRNOM_{3h}$
$C_3H_4O_6$	18	dihydroxy malonic acid	BSTFA	$SRNOM_{3h}$
$C_4H_6O_2$	19		DNPH	$SRNOM_{1h,2\ h,3\ h,4h}$
$C_4H_4O_2$	20	butenedial	DNPH	$SRNOM_{1h,2\ h,3\ h,4h}$
$C_4H_6O_3$	21		DNPH	$SRNOM_{1h,2\ h,3\ h,4h}$
$C_4H_4O_3$	22		DNPH	$SRNOM_{1h,2\ h,3\ h,4h}$
$C_4H_6O_4$	23	butanedioic acid	BSTFA	$SRNOM_{3h}$
$C_4H_4O_4$	24		DNPH	$SRNOM_{1h,2\ h,3\ h,4h}$
$C_4H_6O_5$	25	malic acid	BSTFA	$SRNOM_{3h}$
$C_4H_9NO_2$	26	4-aminobutanoic acid	BSTFA	$SRNOM_{3h}$
$C_5H_8O_4$	27	glutaric acid	BSTFA	$SRNOM_{3h}$
$C_5H_6O_4$	28		DNPH	$SRNOM_{1h,2\ h,3\ h,4h}$
$C_5H_{10}O_5$	29	Xylose	BSTFA	SRNOM
$C_5H_6O_6$	30		DNPH	$SRNOM_{1h,2\ h,3\ h,4h}$
$C_6H_{10}O_4$	31	hexanedioic acid	BSTFA	SRNOM
$C_6H_{12}O_5$	32	L-rhamnose	BSTFA	SRNOM
$C_6H_{12}O_5$	33	fucose	BSTFA	SRNOM
$C_6H_{12}O_6$	34	glucose	BSTFA	SRNOM
$C_6H_{12}O_6$	35	galactose	BSTFA	SRNOM
$C_6H_8O_6$	36		BSTFA	$SRNOM_{3h}$
$C_6H_8O_6$	37	tricarballylic acid	BSTFA	$SRNOM_{3h}$
$C_9H_{16}O_4$	38	azelaic acid	BSTFA	SRNOM
$C_{12}H_{22}O_4$	39	dodecane-dioic acid	BSTFA	SRNOM
$C_{18}H_{34}O_2$	40	oleic acid	BSTFA	SRNOM
$C_{18}H_{36}O_2$	41	stearic acid	BSTFA	$SRNOM_{3h}$

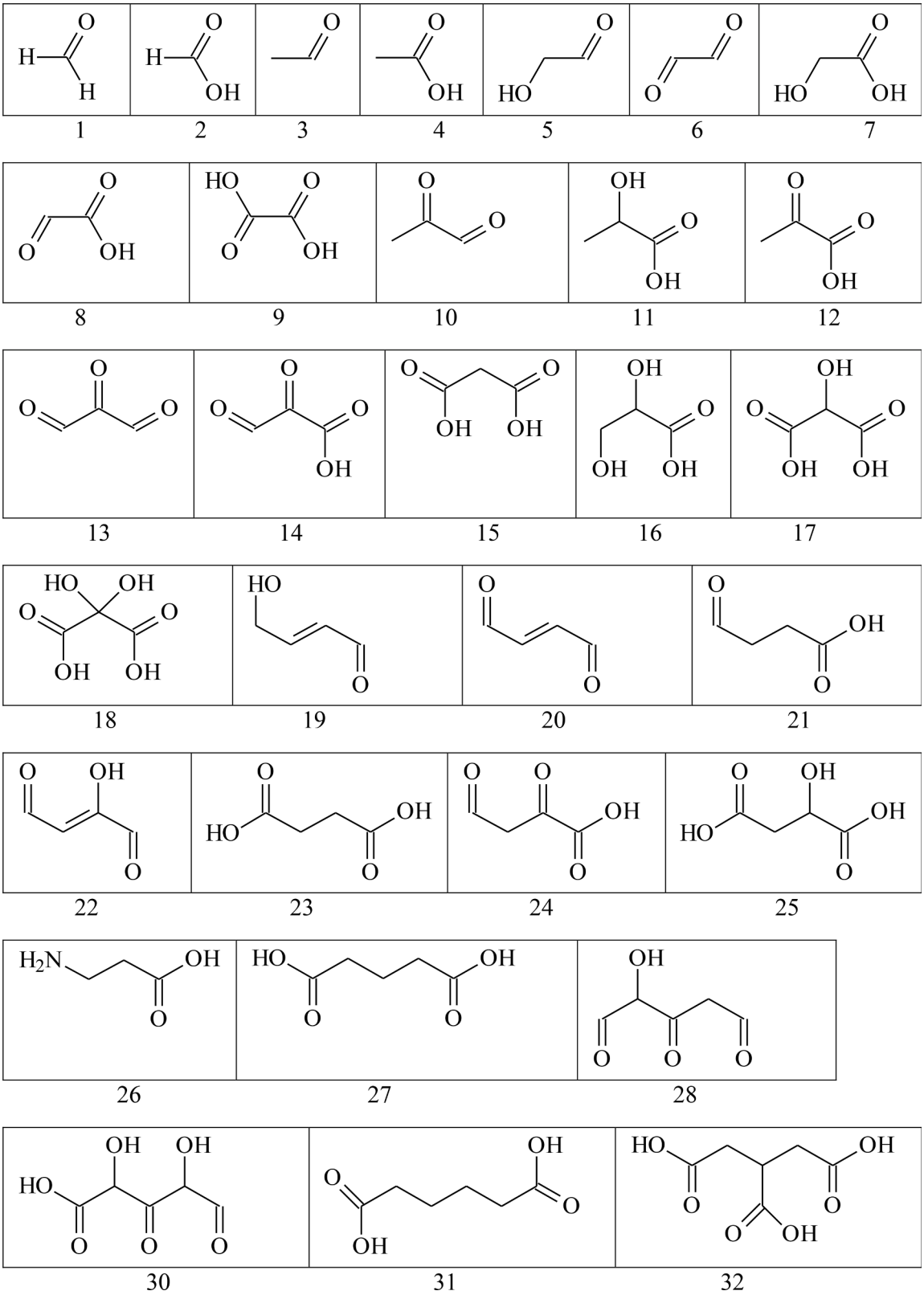

Fig. 2. Carbonyls detected in irradiated SRNOM.

SRNOM photodegradation still proceeds beyond 4 h although a significant absorbance decrease at 254 nm.

The total pool of C_1—C_5 carbonyls was estimated by summing the individual concentrations. Fig. 3B shows that their cumulative concentration increased during the first 2 h of irradiation to reach the value of 2.8×10^{-4} M. Based on these concentrations and on the DOC measurements, the mass percentage of carbon atoms contained in the detected carbonyls could be calculated using Eq (1). This percentage was maximum after 3 h of irradiation where it reached 46% (Fig. 3B). This high value demonstrates the very important contribution of C_1—C_5

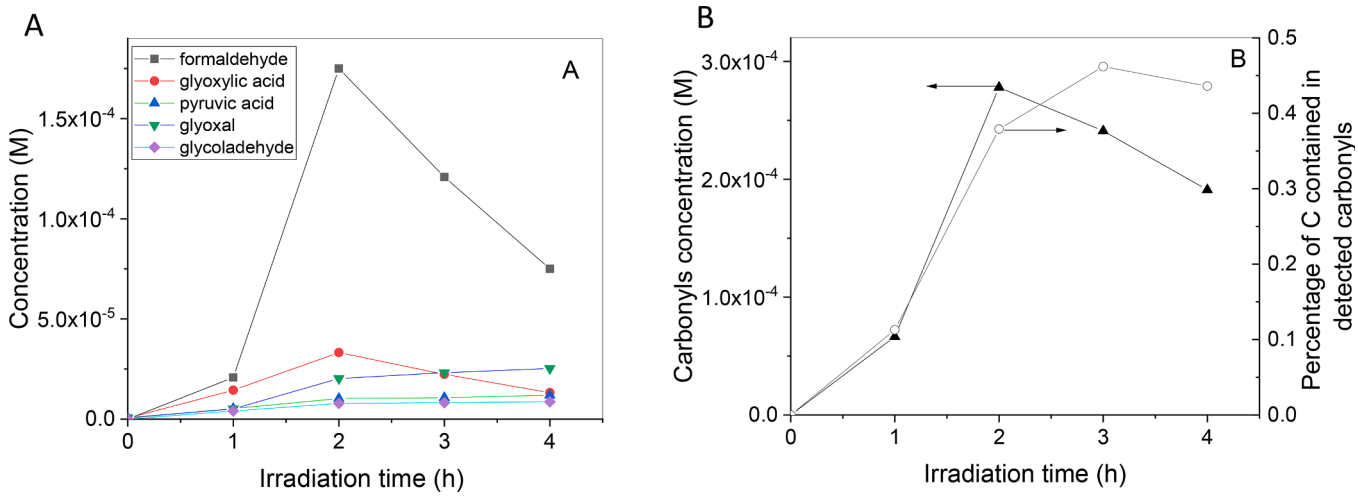

Fig. 3. Evolution of carbonyls detected in irradiated SRNOM by DNPH derivatization. A) Concentration of the main carbonyls vs irradiation time and B) Sum of carbonyls concentration (○, left y-axis) and mass percentage of carbon contained in detected carbonyls (▲, right y-axis) vs irradiation time.

carbonyls to the pool of photoproducts. As most of these compounds poorly absorbed below 300 nm, their high concentration explains the unchanged spectrum shape following irradiation.

$$Mass\ percentage_t = \frac{\sum_{i=1}^{i=n}[c_i]_t \times M_i}{DOC_t} \quad (1)$$

where $[c_i]_t$ and M_i are the concentration at time t and the molecular mass of carbonyl i, and DOC_t is the organic carbon content in the solution at time t.

The concentration of carboxylic acids detected in $SRNOM_{3h}$ are shown in Table SI-5. In general, BSTFA-GC–MS and CI-MS analyses gave consistent results regarding the concentration estimations. BSTFA-GC–MS was however less performant than CI-MS in the analysis of compounds containing 2 or 3 CO_2H or OH functions such as tartronic, dihydroxymalonic acid, oxalic acid and tricarballylic acids. The difficulty to solubilize lyophilized $SRNOM_{3h}$ in acetonitrile to conduct the BSTFA derivatization or a partial derivatization of these compounds probably explain these discrepancies. Malic, oxalic, butanedioic, glycolic, and malonic acids were the most concentrated acids. However, their concentration in $SRNOM_{3h}$ that laid below 2.8×10^{-6} M, were much lower than those of carbonyls. Eq (1) allowed to determine that the detected carboxylic acids contained only 2% in mass of the $SRNOM_{3H}$ carbon atoms.

Nitrate ions were also detected by CI-MS in SRNOM at a level of 2.9×10^{-6} M, but not in $SRNOM_{3h}$.

The detection of all these compounds suggests that the photodegradation of SRNOM under UVC resulted from a complex set of reactions involving the direct photolysis of SRNOM constituents as well as their oxidation by the radicals generated in the course of the irradiation. Many radicals such as R•, RO•, RO_2•, HO_2•/O_2•$^-$ and •OH can be formed by C—C, C—O, and O—O bond cleavage, phenyl-O^- and RCO_2^- photoionization, addition of oxygen on radicals and various radicalar attacks. Once formed, these radicals could contribute to further degradation of SRNOM constituents and of their by-products. Among them, •OH radical is likely to play a significant role for several reasons. It is the most oxidant species able to react with a wide variety of chemicals by addition on double bonds or by H atom abstraction [Buxton et al., 1988]. NOM was shown to generate •OH radicals [Vaughan and Blough, 1998; Page et al., 2011; McKay and Rosario-Ortiz, 2015; Gan et al., 2008; Sun et al., 2015; Dong and Rosario-Ortiz, 2012; Aguer and Richard, 1999] under irradiation. In reactions where •OH radicals are purposely produced [Varanasi et al., 2018] the oxidation degree of photoproducts, given by the O/C ratio, is generally high (1–2), as observed here. Last, the photolysis of chlorosalicylic acid, that was proposed to occur via the intermediary formation of •OH radicals [Tafer et al., 2016], yielded glycolic, lactic, and butanedioic acids, acetaldehyde, glycoaldehyde, methylglyoxal, $C_4H_4O_3$, and $C_3O_3H_2$ that were also detected in the present work.

3.3. Effect of SRNOM pre-irradiation on the oxidant properties at 254 nm

In order to explore the photooxidant properties of pre-irradiated SRNOM, we chose glyphosate as a chemical probe. We first checked that it is photostable when irradiated in our device ($k < 2 \times 10^{-4}$ min^{-1}, Table 3). For these experiments, we selected $SRNOM_{3h}$ that showed the highest concentration of intermediary carbonyl compounds (2.4×10^{-4} M) and SRNOM and $SRNOM_{3h}$ were tested at the same absorbance at 254 nm (0.34). In the presence of SRNOM, glyphosate (10^{-5} M) disappeared with a rate constant k of 0.0013 ± 0.0002 min^{-1} in air-saturated solution (Fig. 4A and Table 3). Making the hypothesis that the reaction was due to the reaction of glyphosate with •OH radicals, we used this rate constant to estimate the quantum yield of •OH radicals formation by SRNOM ($\varnothing_{SRNOM}^{OH}$) in the first stages of the reaction. Once formed by process 1, •OH radicals react with glyphosate ($k_{gly} = (3.37 \pm 0.10) \times 10^7\ M^{-1}\ s^{-1}$, Vidal et al., 2015) (process 2) and with SRNOM (process 3). We took for k_{SRNOM} the value of 1.6×10^8 $M_C^{-1}\ s^{-1}$ reported in the literature for Suwannee river fulvic acid [Westerhff et al., 2007].

$$SRNOM + h\nu \rightarrow SRNOM^* \rightarrow \bullet OH\ (1)\ \varnothing_{SRNOM}^{OH}$$
$$\bullet OH + Glyphosate \rightarrow\ products\ (2)\ k_{Gly}$$
$$\bullet OH + SRNOM \rightarrow\ products\ (3)\ k_{SRNOM}$$

The rate of glyphosate photodegradation (R_{Gly}) can be written (SI-Text 7):

$$R_{Gly} = I_0\left(1 - 10^{-A_{SRNOM}}\right)\varnothing_{OH}^{SRNOM}\frac{k_{gly}\ [Gly]}{k_{gly}[Gly] + k_{SRNOM}\ [SRNOM]} \quad (2)$$

where $I_0\ (1 - 10^{-A_{SRNOM}})$ is the rate of light absorption by SRNOM. As SRNOM was diluted 2.44 fold to reach the same absorbance at 254 nm as $SRNOM_{3h}$, [SRNOM] was equal to 6.35 mgC L^{-1} or 0.529 mM_C^{-1}, taking 12 for the molar mass of carbon. In these conditions, one gets that glyphosate trapped 0.38% of •OH radicals and that $\varnothing_{SRNOM}^{OH}$ was equal to 0.024; this value is in the range of that reported by Lester et al. (2013) at 254 nm (0.047).

In the presence of $SRNOM_{3h}$ and in air-saturated solution, glyphosate disappeared much faster than in the presence of SRNOM (Fig. 4A) with $k = 0.038 \pm 0.004$ min^{-1} (Table 3). In N_2-purged $SRNOM_{3h}$ solution, the glyphosate photodegradation rate was significantly reduced compared

Table 3
First-order rate constants of glyphosate loss, and rates of glyphosate, acetone and pyruvate photodegradation at 254 nm under different conditions.

Conditions	k (min^{-1})	R_{Gly} (M s^{-1})	$R_{acetone}$ (M s^{-1})	$R_{pyruvate}$ (M s^{-1})
Glyphosate alone (10^{-5} M)	$< 2 \times 10^{-4}$	$< 3 \times 10^{-11}$		
+ SRNOM	0.0013 ± 0.0002	2.2×10^{-10}		
+ $SRNOM_{3h}$	0.038 ± 0.004	6.3×10^{-9}		
+ $SRNOM_{3h}$ + 2-propanol (5×10^{-3} M)	0.0036 ± 0.0004	6.0×10^{-10}		
+ $SRNOM_{3h}$ N_2 purged	0.002 ± 0.002	3.3×10^{-10}		
+ H_2O_2 (10^{-5} M)	0.0093 ± 0.001	1.5×10^{-9}		
+ acetone (10^{-4} M)	0.0020 ± 0.001 (0–10 min) 0.024 ± 0.003 (10–30 min)	3.3×10^{-10} (0–10 min) 4.0×10^{-9} (10–30 min)	$< 0.9 \times 10^{-8}$ (0–10 min) 2.4×10^{-8} (10–30 min)	
+ pyruvate (10^{-4} M)	0.021 ± 0.002	3.5×10^{-9}		0.5×10^{-9} (0–6 min) 2.1×10^{-8} (6–30 min)
+ acetone (10^{-4} M) + 2-propanol (10^{-4} M)	0.0050 ± 0.0007	8.3×10^{-10}		
+ pyruvate(10^{-4} M) + 2-propanol (10^{-4} M)	0.0057 ± 0.0008	9.5×10^{-10}		
+ acetone (10^{-4} M) + H_2O_2 (10^{-5} M)	0.016 ± 0.0002	2.7×10^{-9}	1.7×10^{-8}	
acetone alone (2.4×10^{-4} M)			$< 0.9 \times 10^{-8}$ (0–10 min) 3.9×10^{-8} (10–30 min)	
+ H_2O_2 (10^{-5} M)			3.5×10^{-8}	
+ H_2O_2 (10^{-3} M)			1.8×10^{-7}	

to the one conducted in air-saturated medium ($k = 0.002 \pm 0.002$ min^{-1} in the first 10 min of the reaction, Fig. 4A, Table 3) demonstrating the important role played by oxygen in the reaction. Moreover, we irradiated glyphosate and $SRNOM_{3h}$ in the presence of 2-propanol to determine whether •OH radicals were involved in the loss of glyphosate. Using $k_{2\text{-}propanol} = 1.9 \times 10^9$ M^{-1} s^{-1} [Buxton et al., 1988] for the bimolecular rate constant of reaction between •OH and 2-propanol:

•OH + 2-propanol → products (4) $k_{2\text{-}propanol}$

we added 5×10^{-3} M of 2-propanol expecting an inhibition of the reaction > 90% based on $k_{SRNOM3h}[SRNOM_{3h}] \sim 9 \times 10^4$ s^{-1}, as for SRNOM. The inhibition was of 90% (Fig. 4A, Table 3) in accordance with a significant contribution of •OH.

Spin trap experiments using DMPO as the spin-trapping reagent were also conducted to confirm the formation of •OH radicals. Fig. 5 shows that the four-line signal with an intensity ratio 1:2:2:1 characteristic of the DMPO—OH• adduct was not detected when DMPO was irradiated in the presence of SRNOM (plot a) or H_2O_2 (10^{-5}) (plot c) while it was observed with $SRNOM_{3h}$ (plot b) and H_2O_2 (5×10^{-3} M) (plot d). Again, this result is in line with the production of •OH radicals upon irradiation of $SRNOM_{3h}$ in UVC.

Postulating that the disappearance of glyphosate was only due to the reaction with •OH, we made the same calculation for $SRNOM_{3h}$ as for SRNOM, after having replaced processes 1 and 2 by processes 1′ and 3′ respectively:

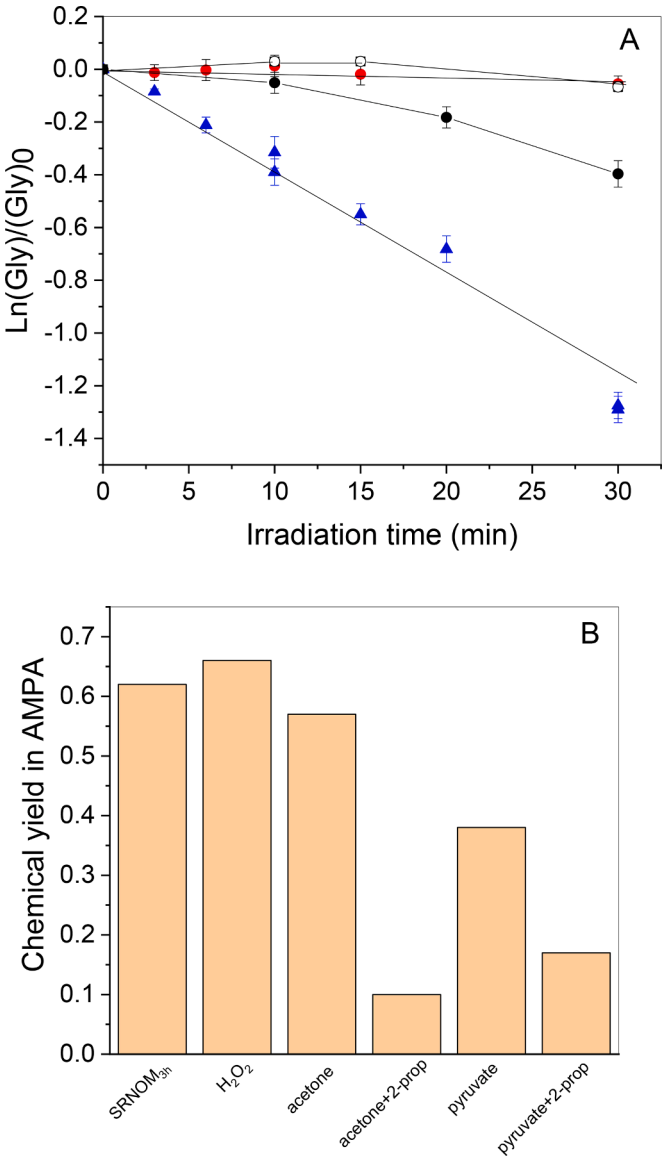

Fig. 4. Loss of glyphosate (10^{-5} M) (A) and formation of AMPA (B) under irradiation at 254 nm in presence of SRNOM (●), $SRNOM_{3h}$ (●), $SRNOM_{3h}$ + 2-propanol (5×10^{-3} M) (○), and $SRNOM_{3h}$ in N_2-saturated medium (●). A_{254} of SRNOM and $SRNOM_{3h}$ is equal to 0.34 in a cuvette and 0.68 in the reactor.

$SRNOM_{3H} + h\nu \rightarrow SRNOM_{3H}^* \rightarrow$ •OH (1') $\varnothing_{SRNOM}^{OH}$
•OH + $SRNOM_{3H}$ → products (3') $k_{SRNOM3h}$

and substituting SRNOM by $SRNOM_{3h}$ in Eqn 2. The TOC analyses showed that $SRNOM_{3h}$ had a DOC content of 10.9 mgC L^{-1} or 0.907 mM_C^{-1} (Table 1). To estimate the percentage of •OH radicals reacting with glyphosate in $SRNOM_{3h}$ solution, we also need to know the value of $k_{SRNOM3h}$. Since $SRNOM_{3h}$ is much less aromatic than SRNOM, and •OH radicals react more easily with aromatic or conjugated structures than with saturated ones, $k_{SRNOM3h}$ is possibly smaller than k_{SRNOM}. Postulating that the rate constant decrease may parallel the absorbance decrease at 254 nm, we opted for $k_{SRNOM3h} = (0.7 \pm 0.3) \times 10^8$ M_C^{-1} s^{-1}. From this value, the percentage of •OH radicals trapped by glyphosate in $SRNOM_{3h}$ solution would lay between 0.3 and 0.8% and $\varnothing_{SRNOM3h}^{OH}$ would be comprised between 0.21 and 0.55, a value between 10 and 20 times higher than that found for $\varnothing_{SRNOM}^{OH}$. This value must be considered as a maximal value and would be lower if radicals other than •OH also contributed to the degradation of glyphosate. To better understand the

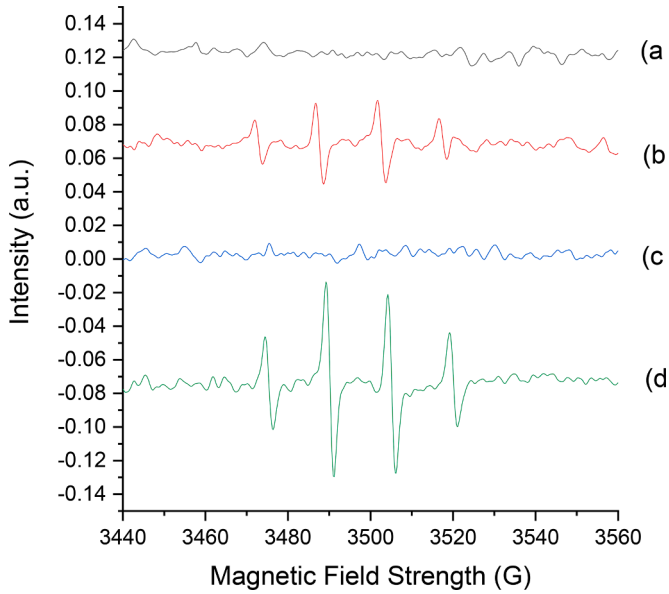

Fig. 5. ESR spectra obtained upon irradiation of DMPO (25 mM) in the presence of SRNOM (20 mg L^{-1}) (a), $SRNOM_{3h}$ (b), H_2O_2 (10^{-5} M) (c) and H_2O_2 (5 × 10^{-3} M) (d).

enhancing effect of the pre-irradiation on the photooxidant properties of SRNOM, we conducted additional experiments and tested potential candidates for their ability to photodegrade glyphosate.

3.4. Peroxides formation and role of H_2O_2 in the oxidant properties at 254 nm

Peroxides are sources of •OH radicals through direct photolysis (process 5) or photo-Fenton reaction and we quantified their formation in our system. Measurements of H_2O_2 and RO_2H + RO_2R were performed on SRNOM and $SRNOM_{3h}$ irradiated for 30 min (Fig. 5). In SRNOM, H_2O_2 and RO_2H + RO_2R accumulated linearly. After 30 min of irradiation, the total concentration of H_2O_2 + RO_2H + RO_2R was equal to 16 μM; H_2O_2 was by far the most abundant species (14.2 μM) while RO_2H + RO_2R contributed to the pool of peroxides in a minor way (1.8 μM). In $SRNOM_{3h}$, the peroxides formation was auto-inhibited, slowing down after 10 min. The total concentration reached 15.8 μM after 30 min; H_2O_2 and RO_2H + RO_2R were in equivalent amounts of ~ 8.0 μM. The formation of H_2O_2 in the photolysis of NOM is well documented in the literature [Garg et al., 2011]. It is formed by dimutation of $O_2^{\bar{}}$ that arises from reduction of dissolved O_2. Peroxides and hydroperoxides are generated after the reaction of R· radicals with dissolved O_2 to yield $RO_2^{\cdot}$ and the reaction of these peroxyl radicals with $O_2^{\bar{}}/HO_2^{\cdot}$ [Sun et al., 2021].

To determine the contribution of H_2O_2 to the formation of •OH via process (5), we proceeded as follows. We first measured R_{Gly} in the presence of H_2O_2 (10^{-5} M) alone. The value of 1.5 × 10^{-9} M^{-1} s^{-1} allowed us to check that glyphosate reacted with •OH and to measure the photon flux I_0 in the irradiation device (SI-Text 1). Then, we calculated R_{Gly}^{H2O2} in SRNOM solution using Eq (3), supposing that the photolysis of H_2O_2 produced during the irradiation of SRNOM was the only source of •OH through process 5 (SI-Text 5).

$H_2O_2 \rightarrow$ •OH $\varnothing_{H2O2}^{OH}$ (5)

$$R_{Gly}^{H2O2} = I_{a,H2O2}^{SRNOM}\ \varnothing_{H2O2}^{OH} \frac{k_{gly}\ [Gly]}{k_{gly}[Gly] + k_{SRNOM}\ [SRNOM] + k_{H2O2}\ [H_2O_2]} \quad (3)$$

Taking $[H_2O_2]$ = 14 μM (corresponding to the highest value reached for SRNOM), ε_{H2O2} = 19.6 M^{-1} cm^{-1} at 254 nm, A_{254} = 0.34 for SRNOM and ℓ = 2, we calculated $I_{a,H2O2}^{SRNOM}$ using the Beer-Lamber law for a mixture (SI-Text 8). Then, taking k_{H2O2} = 2.7 × 10^7 $M^{-1}.s^{-1}$ [Stefan et al., 1996], we got that glyphosate trapped 0.38% of •OH and using $\varnothing_{H2O2}^{OH}$ = 1 [Yu and Barker, 2003], we finally obtained R_{Gly}^{H2O2} = 7.0 × 10^{-12} M s^{-1}. In the case of $SRNOM_{3h}$, we took $[H_2O_2]$ = 8 μM and the same calculation led to R_{Gly}^{H2O2} = (3.0–9.0) × 10^{-12} M s^{-1}. Both values are very small compared to the experimental values 2.2 × 10^{-10} M s^{-1} and 6.5 × 10^{-9} M s^{-1} respectively measured for SRNOM and $SRNOM_{3h}$ and it can be concluded that the photochemical decomposition of titrated hydroperoxides negligibly contributed to the oxidation of glyphosate. Spontaneous decomposition of unstable hydroperoxides into RO• and •OH might be an alternative source of •OH radicals. This was considered by Badali et al. (2015) and Krapf et al. (2016) in their studies on secondary organic aerosols.

3.5. Role of carbonyls in the photooxidant properties at 254 nm

Given the high concentration of carbonyls detected in $SRNOM_{3h}$ and the known potential of these chemicals as sensitizers, we tested if they could induce the transformation of glyphosate at 254 nm. We first tested pyruvic acid since this compound had been previously detected in our irradiated SRNOM samples. In the presence of this ketoacid (10^{-4} M), in pH 7 buffered solutions, glyphosate (10^{-5} M) disappeared with an apparent first order rate constant equal to 0.021 ± 0.002 min^{-1} (Fig. 6A, Table 3). Pyruvate was also photodegraded and the reaction auto-accelerated. During the first 6 min of irradiation, only 1.8 × 10^{-6} M of pyruvate were transformed against 3.1 × 10^{-5} M between 6 and 30 min (Fig. 6B). The rate of pyruvate loss, $R_{pyruvate}$, in the second part of the curve was equal to 2.1 × 10^{-8} M s^{-1}, and R_{Gly} to 3.5 × 10^{-9} M s^{-1}. The experiment was repeated in the presence of 2-propanol added to trap •OH radicals. The concentration 10^{-4} M was chosen for 2-propanol for a theoritical trapping of more than 95% based on $k_{pyruvate\ acid}$ = 3 × 10^8 M^{-1} s^{-1} (process 6) [Buxton et al., 1988]. After 30 min, the rate of glyphosate loss was reduced by 75% confirming a significant contribution of •OH in the reaction.

•OH + pyruvate → products (6) $k_{pyruvate}$

Although it was not detected in irradiated SRNOM samples, acetone

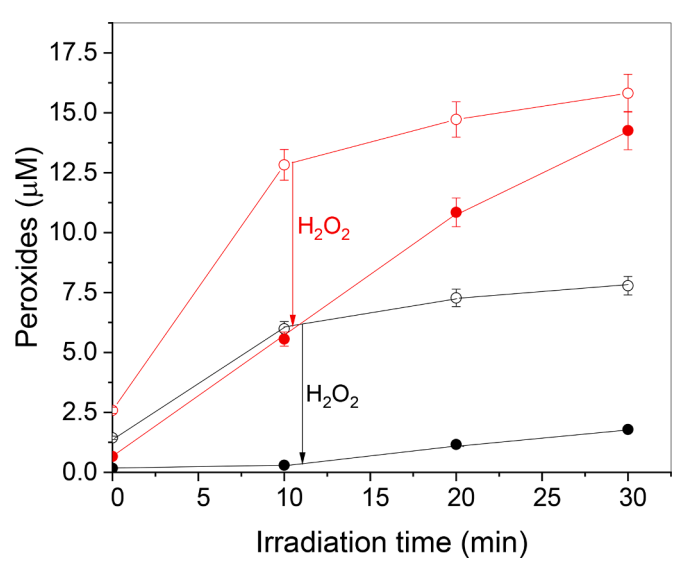

Fig. 6. Formation of peroxides upon irradiation of SRNOM at 254 nm. H_2O_2 + ROOR + ROOH in SRNOM (●) and in $SRNOM_{3h}$ (○); ROOR + ROOH in SRNOM (●) and in $SRNOM_{3h}$ (○).

was chosen to represent monocarbonyls because it is a simple molecule, it can be purchased in high purity, it was already studied and its quantum yield of photolysis is known ($\varnothing_{acetone} = 0.061$ at 270 nm, Anpo and Kubokawa, 1977). At 10^{-4} M, a concentration falling within the range of that found for intermediary carbonyls, acetone increased the rate of glyphosate photodegradation and the reaction was also auto-accelerated (Fig. 6A, Table 3). During the first 10 min of reaction, an averaged $k = 0.002 \pm 0.001$ min^{-1} was obtained while, between 10 and 30 min, we measured $k = 0.024 \pm 0.003$ min^{-1}. In parallel, the decay of acetone was monitored by UHPLC—HRMS after DNPH derivatization. Acetone also disapppeared by an autoaccelerated reaction (Fig. 6B). Between 0 and 10 min, the loss of acetone was lower than 5% corresponding to a rate of acetone photodegradation ($R_{acetone}$) $< 0.9 \times 10^{-8}$ M s^{-1} while, between 10 and 40 min, acetone disappeared by 43% and $R_{acetone}$ was equal to 2.4×10^{-8} M s^{-1} (Table 3). During this reaction H_2O_2 was formed (Fig. 6B). The H_2O_2 production was of 2 μM between 0 and 10 min and 10 μM between 10 and 30 min which mirrored the autoaccelerated decrease of glyphosate and acetone. In the presence of 2-propanol (10^{-4} M) and acetone (10^{-4} M), glyphosate disappeared by 10% instead of 42% in the absence of 2-propanol after 30 min of irradiation (Fig. 6A, Table 3) confirming again a significant contribution of •OH in the reaction (75%).

Acetone was also irradiated alone to check that the observed autoacceleration was not due to the presence of glyphosate. At 2.4×10^{-4} M, acetone also disappeared in an auto-accelerated reaction with $R_{acetone} < 0.9 \times 10^{-8}$ M^{-1} s^{-1} between 0 and 10 min and $R_{acetone} = 3.9 \times 10^{-8}$ M^{-} s^{-1} between 10 and 30 min (Table 3). The photoproducts were pyruvic acid, methyl glyoxal, hydroxyacetone, formadehyde as described by Stefan and Bolton (1999) when they studied the photolysis of acetone in the presence of H_2O_2 at 254 nm. Using the quantum yield of acetone photodegradation in diluted solutions (0.061), and $\varepsilon_{\text{acetone}} = 16$ M^{-1} cm^{-1} at 254 nm, it is possible to calculate the rate of acetone photodegradation by direct photolysis $R^{dp}_{acetone}$ using EQ. 4:

$$R^{dp}_{acetone} = I_0\left(1 - 10^{-A_{acetone}}\right)\varnothing_{acetone} \quad (4)$$

For [acetone]$= 10^{-4}$ M, one gets $R^{dp}_{acetone} = 1.3 \times 10^{-9}$ M s^{-1} and for [acetone]$= 2.4 \times 10^{-4}$ M $R^{dp}_{acetone} = 3.1 \times 10^{-9}$ s^{-1}. These values are consistent with the ones obtained between 0 and 10 min ($< 9 \times 10^{-9}$ M s^{-1}), and one can conclude that $R^{dp}_{acetone}$ being negligible behind $R_{acetone}$ measured in the second part of the curves, other reactions should take place.

An autoaccelerated reaction is generally due to the accumulation of key intermediates. Here, the intermediary chemicals were the acetone photoproducts and peroxides, among which, H_2O_2. We therefore studied the effect of H_2O_2, used a hydroperoxide model, at the concentration of 10^{-5} and 10^{-3} M on the photodegradation of acetone (2.4×10^{-4} M). The photodegradation of acetone was fast till the very beginning of the irradiation ($R_{acetone} = 3.5 \times 10^{-8}$ and 1.8×10^{-7} M s^{-1}, respectively, Table 3) and no auto-accelerating effect was observed. In this mixture, acetone can disappear by reaction with •OH produced from H_2O_2 photolysis (process 7, $k_{acetone} = 1.1 \times 10^8$ M^{-1} s^{-1}, Buxton et al., 1988). Process 8 is a potential competiting pathway of •OH disappearance ($k_{H2O2} = 2.7 \times 10^7$ M^{-1} s^{-1} Buxton et al., 1988).

•OH + acetone → products (7) $k_{acetone}$
•OH + H_2O_2 → products (8) k_{H2O2}

For [H_2O_2] $= 10^{-3}$ M and [acetone] $= 2.4 \times 10^{-4}$ M, process 8 was expected to significantly reduce the percentage of •OH radicals trapped by acetone. Taking into account that acetone should trap about 50% of •OH, one obtains $R_{acetone} = 1.3 \times 10^{-7}$ M.s^{-1} against 1.8×10^{-7} M s^{-1} measured experimentally. For [H_2O_2] $= 10^{-5}$ M and [acetone] $= 2.4 \times 10^{-4}$ M, process 8 was negligible, and acetone was expected to trap all the •OH radicals produced by H_2O_2 photolysis. Its rate of decay through process 7 ($R^{OH}_{acetone}$) was equal to 2.6×10^{-9} M s^{-1} according to EQ (5).:

$$R^{OH}_{acetone} = I_0\left(1 - 10^{-A_{H2O2}}\right)\varnothing^{OH}_{H2O2} \quad (5)$$

This calculated rate accounted for only 6.6% of the measured rate indicating that an additional radical source was responsible for acetone degradation. Then, we simultaneously irradiated glyphosate (10^{-5} M), H_2O_2 (10^{-5} M) and acetone (10^{-4} M). In this case, the glyphosate photodegradation was fast till the beginning of the irradiation ($k = 0.016$ min^{-1}) (Fig. 6A, Table 3) showing that H_2O_2 or other hydroperoxides are important intermediaries in the reaction.

The results obtained for acetone can be tentatively explained by the chain-reaction mechanism shown in Scheme 1. In the classical chain oxidation of a chemical RH bearing a labile H atom, the initiator produces the primary radicals (process 9) that start the chain through a transfer reaction by generating the radical R• (process 7). Then R• produces RO_2• by adding O_2 (process 10) and RO_2• regenerates R• along to RO_2H by abstracting of a H from RH (process 11). The longer the chain length, the faster the reaction; in fact, when the chain is long enough, the rate of the propagation reactions becomes much higher than the rates of initiation and of transfer. In our case, the calculated rate of acetone photolysis $R^{dp}_{acetone}$ (process 9) was much lower than the experimental rate of acetone photodegradation consistently with the involvement of a chain reaction.

The irradiation of acetone was expected to yield radicals by α-cleavage of the triplet excited state (process 9) [Pearson, 1963]. The triplet could also abstract a H-atom from methyl groups of acetone, however, neither acetone itself nor glyphosate were concentrated enough to compete significantly with the cleavage [Anpo and Kubokawa, 1977]. Due to the oxidation of these radicals and to the photolysis of the formed hydroperoxides, there should be a pool of initiating radicals in the system. The acetonyl radical, R•, formed by process 7 [Stefan et al., 1996] should easily react with oxygen (process 10) to yield the peroxyl radical ROO• [Stefan et al., 1996]. This peroxyl radical likely abstracted an H-atom from acetone (process 11) to regenerate the acetonyl radical and produce the hydroperoxide ROOH. The recombination of two peroxide radicals (process 12) terminated this chain reaction.

In this chain reaction, glyphosate might be oxidized by several of the radicals formed in the complex mixture. However, while the reaction with •OH was evidenced, the oxidation with the other radicals remains to be demonstrated. If we make the hypothesis that •OH contributed significantly to the glyphosate degradation, the source of •OH needs to be explained. Indeed, calculations showed that the photolysis of the different hydroperoxides did not yield enough radicals to explain the high rate of glyphosate degradation. An alternative formation of •OH could be the spontaneous decomposition at room temperature of unstable hydroperoxides, here CH_3—CO—CH_2OOH (process 13). According to the works of Badali et al. (2015) and Krapf et al. (2016), the formation of very unstable hydroperoxides is plausible. Therefore, despite processes 7, 10 and 11 still taking place, the key process became process 13 since it introduced a continuous source of •OH and RO• radicals. Consequently, the rate of glyphosate degradation increased during the accumulation phase of ROOH, reaching the maximal value rate when the RO_2H formation equaled the RO_2H decomposition.

CH_3—CO—CH_2OOH → CH_3—CO—CH_2O• + •OH (13)

In the case of $SRNOM_{3h}$, carbonyls were present at 2.4×10^{-4} M and hydroperoxides were potentially generated at a fast rate, therefore making it possible the mechanism already proposed in the case of acetone to occur. In accordance, ROOH + ROOR were formed along with H_2O_2. In $SRNOM_{3h}$ solution, R_{gly} was equal to 6.3×10^{-9} M s^{-1}. Considering that glyphosate trapped between 0.3 and 0.8% of •OH radicals in competition with $SRNOM_{3H}$ constituents, the rate of •OH formation should be comprised between $\sim 8 \times 10^{-7}$ and 2×10^{-6} M s^{-1}. In the model solution containing glyphosate (10^{-5} M), H_2O_2 (10^{-5} M) and acetone (10^{-4} M), R_{gly} was equal to 2.7×10^{-9} M s^{-1}.

Considering that •OH contributed to the reaction at 75% and that glyphosate trapped 3% of •OH in competition with acetone, then the rate of •OH formation should be equal to $\sim 7 \times 10^{-8}$ M s^{-1}. For acetone (2.4×10^{-4} M), it might be $\sim 1.7 \times 10^{-7}$ M s^{-1}. This value is smaller than that estimated for the $SRNOM_{3h}$ solution, and several explanations of this difference can be proposed: (i) $SRNOM_{3h}$ was a much more complex system than H_2O_2 + acetone and quantitative results cannot be directly transferable; furthermore, calculation lays on an hypothetical value of the bimolecular reaction rate constant of $SRNOM_{3h}$ with •OH; (ii) Acetone was chosen as a model compound but among the carbonyls formed in $SRNOM_{3h}$, some may absorb more than acetone, especially those bearing double bonds, and/or photodissociate much more easily [Anpo and Kubokawa, 1977]; (iii) $SRNOM_{3h}$ also contained chemicals acting probably as better H-donors than acetone and glyphosate, which should favor process 11 and thus the formation of unstable hydroperoxides; (iv) Oxidant species other than •OH might contribute to the photodegradation of glyphosate.

In the case of SRNOM, R_{Gly} was much higher than R_{Gly}^{H2O2} as for $SRNOM_{3h}$ suggesting that chain reactions might take place as for $SRNOM_{3_h}$, although leading to a much slower production of •OH. Accordingly, the 6-times less formation of ROOR+ROOH from SRNOM than from $SRNOM_{3h}$ suggests that unstable hydroperoxides should be produced in smaller amounts by SRNOM than by $SRNOM_{3h}$. Spectral measurements showed that SRNOM is much more aromatic than $SRNOM_{3h}$ which constitutes an important difference in terms of •OH reactions. The •OH radicals are known to add on phenols [Lundquist and Eriksson, 2000] to finally produce unreactive phenoxyl radicals while they generate radicals oxidable into hydroperoxides when they abstract hydrogen atoms from aliphatic compounds. Hence, the presence of carbonyls in $SRNOM_{3h}$ could not only favor the formation of radicals through their photolysis but also constitutes a pool of aliphatic compounds oxidable into hydroperoxides.

AMPA was the main glyphosate photoproduct detected by UHPLC—HRMS (Fig. 4B). In the literature, other oxidation products were also detected such as sarcosine [Chen et al., 2007], not detected in this work. After 30 min of irradiation, the highest yield of AMPA was measured with H_2O_2 (66%), followed by $SRNOM_{3h}$ (62%), acetone (57%) and pyruvic acid (38%). Interestingly, when 2-propanol was added to acetone and pyruvate solutions, the yield of AMPA dropped to 10% and 17%, respectively. The formation of AMPA may be thus an indirect evidence of the involvement of •OH radicals in the photodegradation.

Fig. 7.

3.5. Effect of SRNOM pre-irradiation on •OH, $^1O_2$ and $^3SRNOM^*$ formation under simulated solar light

We also compared the ability of SRNOM and $SRNOM_{3h}$ to photoproduce photooxidants 3SRNOM*, 1O2 and •OH in simulated solar-light. After the normalization for light absorption, the rate of 2,4,6-trimethyphenol was found to be 1.5 times higher in SRNOM than in $SRNOM_{3H}$, in accordance with lower rate of ^{3}SRNOM* formation. Therefore, chromophores yielding ^{3}SRNOM* were partly degraded under UVC irradiation. In the case of $^1O_2$ titrated using furfuryl alcohol, we found rates of formation varying by less than 10% between SRNOM and $SRNOM_{3h}$. At last, results on terephthalic acid used to estimate the rate of •OH formation showed a higher rate of •OH formation in $SRNOM_{3h}$ solution than in SRNOM solution. Taking $k_{SRNOM} = 1.6 \times 10^8$ M_C^{-1} s^{-1} and $k_{SRNOM3h} = 0.7 \times 10^8$ M_C^{-1} s^{-1} for the bimolecular rate constants of reaction with •OH, we got a rate of •OH formation higher by 40% for $SRNOM_{3h}$ solution than for SRNOM solution. This enhancement was much lower than the one observed at 254 nm with glyphosate. The dependence of the •OH formation enhancement on the irradiation wavelength supports the hypothesis of the involvement of poorly conjugated and light absorbing carbonyl compounds in the photochemical production of •OH.

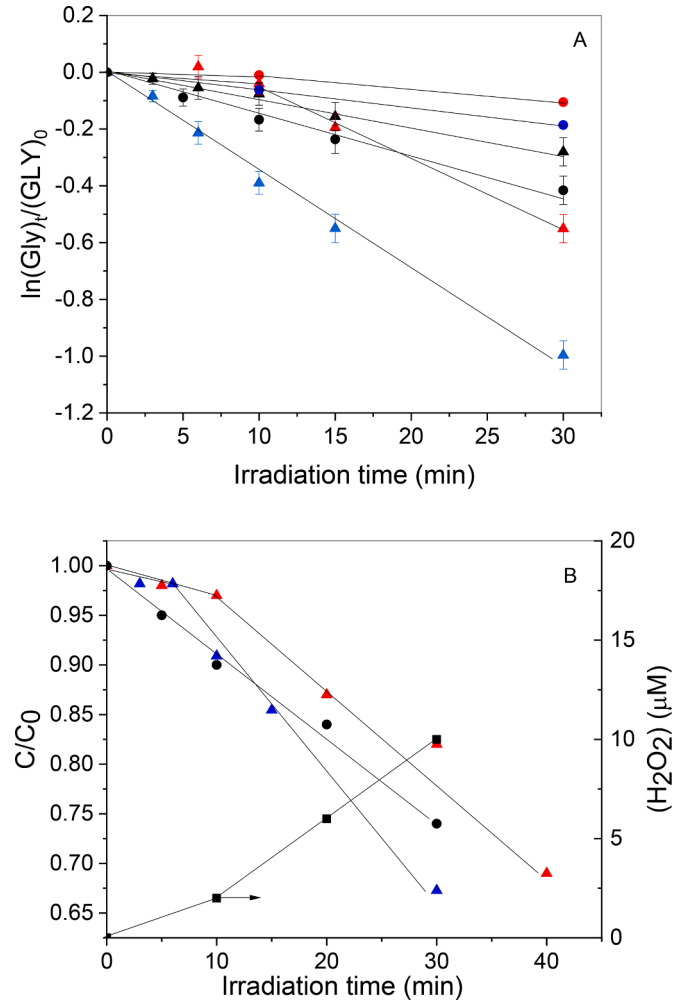

Fig. 7. Photolysis of glyphosate (10^{-5} M) (A) in the presence of H_2O_2 (10^{-5} M) (▲), acetone (10^{-4} M) (▲), acetone (10^{-4} M) + H_2O_2 (10^{-5} M) (●), pyruvate (10^{-4} M) (▲), acetone (10^{-4} M) + 2-propanol (10^{-4} M) (●) and pyruvate (10^{-4} M) + 2-propanol (10^{-4} M) (●). B: loss of acetone (▲, ●), of pyruvate (■), and formation of H_2O_2 (■). Solutions buffered at pH 7.

4. Conclusion

This work aimed to investigate the effect of UVC irradiation on the ability of SRNOM to generate oxidant species, in particular •OH radicals under UVC. Through in-depth analytical and kinetic studies, we demonstrated that SRNOM irradiation drastically increased the pool of aliphatic carbonyls together with its capacity of photoinducing the degradation of glyphosate at 254 nm. Several experimental results suggest that •OH radicals contributed to this degradation. To better understand the role of carbonyls in the reaction, we studied the photodegradation of glyphosate in the presence of acetone and pyruvate. Experimental data were explained by a mechanism involving a chain reaction in which •OH radicals may be formed through the spontaneous decomposition of unstable hydroperoxides. The same mechanism might prevail in pre-irradiated SRNOM and explain its high efficiency to photodegrade glyphosate upon irradiation at 254 nm. These results show that in UVC treatments NOM could favor the degradation of micropollutants through its high capacity to generate very oxidant radicals. Such a pretreatment of NOM would deserve to be further studied in combination with other engineered water treatment sytems.

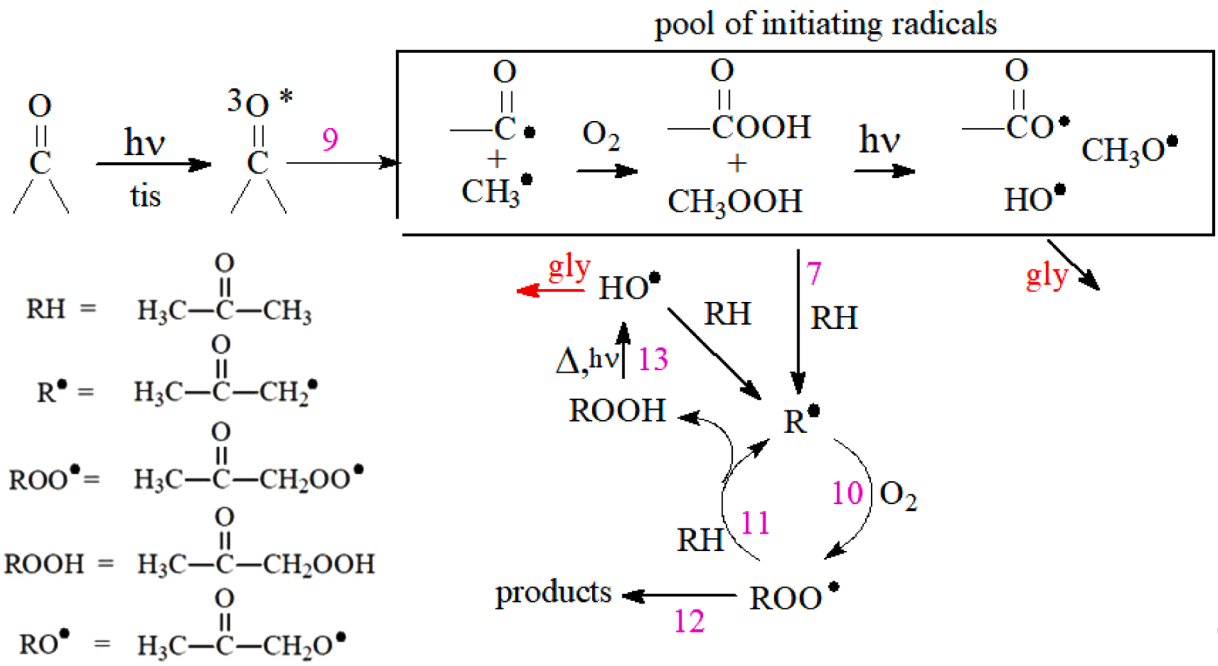

Scheme 1. Mechanism of photodegradation of acetone at 254 nm. In red, in the presence of glyphosate.

Declaration of Competing Interest

The authors declare that they have no known competing financial interests or personal relationships that could have appeared to influence the work reported in this paper.

Acknowledgments

This paper is part of a project that received funding from the European Union's Horizon 2020 research and innovation program under the Marie Skłodowska-Curie grant agreement no. 765860 (Aquality). The authors would like to thank Martin Leremboure (Engineer CNRS) and Frédéric Emmenegger (Tech CNRS) for UHPLC-MS analyses and Lawrence Frezet (Engineer CNRS) for ESR experiments.

Supplementary materials

Supplementary material associated with this article can be found, in the online version, at doi:10.1016/j.watres.2021.117395.

References

Agbaba, J., Jazic, J.M., Tubic, A., Watson, M., Maletić, S., Kragulj Isakovski, M., Dalmacija, B., 2016. Oxidation of natural organic matter with processes involving O3, H2O2 and UV light: formation of oxidation and disinfection by-products. RSC Adv. 6, 86212–86219. https://doi.org/10.1039/C6RA18072H.

Aguer, J.P., Richard, C., 1999. Influence of the excitation wavelength on the photoinductive properties of humic substances. Chemosphere 38, 2293–2301. https://doi.org/10.1016/S0045-6535(98)00447-0.

Anpo, M., Kubokawa, Y., 1977. Reactivity of excited triplet alkyl ketones in solution. I. quenching and hydrogen abstraction of triplet acetone. Bull. Chem. Soc. Jpn. 1977 (50), 1913. https://doi.org/10.1246/bcsj.50.1913.

Badali, K.M., Zhou, S., Aljawhary, D., Antiñolo, M., Chen, W.J., Lok, A., Mungall, E., Wong, J.P.S., Zhao, R., Abbatt, J.P.D., 2015. Formation of hydroxyl radicals from photolysis of secondary organic aerosol material. Atmos. Chem. Phys. 15, 7831–7840. https://doi.org/10.5194/acp-15-7831-2015.

Brinkmann, T., Horsch, P., Sartorius, D., Frimmel, F.H., 2003. Photoformation of low molecular weight organic acids from brown water dissolved organic matter. Environ. Sci. Technol. 37, 4190–4198. https://doi.org/10.1021/es0263339.

Buchanan, W., Roddick, F., Porter, N., 2016. Formation of hazardous by-products resulting from the irradiation of natural organic matter: comparison between UV and VUV Irradiation. Chemosphere 63 (7), 1130–1141. https://doi.org/10.1016/j.chemosphere.2005.09.040.

Buxton, G.V., Greenstock, C.L., Helman, W.P., Ross, A.B., 1988. Critical review of rate constants fro reactions of hydrated electrons, hydrogen atoms and hydroxyl radicas in aqueous solution. J. Phys. Chem. Ref. Data 17, 513–886. https://doi.org/10.1063/1.555805.

Chen, Y., Wu, F., Lin, Y., Deng, N., Bazhin, N., Glebov, E., 2007. Photodegradation of glyphosate in the ferrioxalate system. J. Hazard. Mat. 148, 360–365. https://doi.org/10.1016/j.jhazmat.2007.02.044.

Corin, N., Backlund, P., Kulovaara, M., 1996. Degradation products formed during UV-irradiation of humic waters. Chemosphere 33, 245–255. https://doi.org/10.1016/0045-6535(96)00167-1.

de Bryun, W.J., Clark, C.D., Pagel, L., Takehara, C., 2011. Photochemical production of formaldehyde, acetaldehyde and acetone from chromophoric dissolved organic matter in coastal waters. J. Photochem. Photobiol. A 226, 16–22. https://doi.org/10.1016/j.jphotochem.2011.10.002.

Dong, M.M., Rosario-Ortiz, F.L., 2012. Photochemical formation of hydroxyl radical from effluent organic matter. Environ. Sci. Technol. 46, 3788–3794. https://doi.org/10.1021/es2043454.

Fukushima, M., Tatsumi, K., 2001. Degradation characteristics of humic acid during photo-fenton processes. Environ. Sci. Technol. 35, 3683–3690. https://doi.org/10.1021/es0018825.

Gan, D., Jia, M., Vaughan, P.P., Falvey, D.E., Blough, N.V., 2008. Aqueous Photochemistry of Methyl-Benzoquinone. J. Phys. Chem. A 112, 2803–2812. https://doi.org/10.1021/jp710724e.

Garg, S., Rose, A.L., Waite, T.D., 2011. Photochemical production of superoxide and hydrogen peroxide from natural organic matter. Geochim. Cosmochim. Acta 75, 4310–4320. https://doi.org/10.1016/j.gca.2011.05.014.

Goldstone, J.V., Pullin, M.J., Bertilsson, S., Voelker, B.M., 2002. Reactions of hydroxyl radicals with humic substances: bleaching, mineralization and production of bioavailable carbon substrates. Environ. Sci. Technol. 36, 364–372. https://doi.org/10.1021/es0109646.

Hao, W., Zhanghao, C., Feng, S., Jingyi, L., Xin, J., Chao, W., Cheng, G., 2020. Characterization for the transformation of dissolved organic matters during ultraviolet disinfection by differential absorbance spectroscopy. Chemosphere 243, 125374. https://doi.org/10.1016/j.chemosphere.2019.125374.

Ike, I.A., Karanfil, T., Cho, J., Hur, J., 2019. Oxidation byproducts from the degradation of dissolved organic matter by advanced oxidation processes -A critical review. Water Res 164, 114929. https://doi.org/10.1016/j.watres.2019.114929.

Kieber, R.J., Zhou, X., Mopper, K., 1990. Formation of carbonyl compounds from UV-induced photodegradation of humic substances in natural waters: fate of riverine carbon in the sea. Limnol. Oceanogr. 35, 1503–1515. https://doi.org/10.4319/lo.1990.35.7.1503.

Krapf, M., Haddad, I.E., Bruns, E.A., Molteni, U., Daellenbach, K.R., Prevot, A.S.H., Baltensperger, U., Dommen, J., 2016. Labile peroxides in secondary organic. Aerosol. Chem. 1, 603–616. https://doi.org/10.1016/j.chempr.2016.09.007.

Kulovaara, M., Corin, N., Backlund, P., Tervo, J., 1996. Impact of UV_{254}-irradiation on aquatic humic substances. Chemosphere 33, 783–790. https://doi.org/10.1016/0045-6535(96)00233-0.

Lamsal, R., Walsh, M.E., Gagnon, G.A., 2011. Comparison of advanced oxidation processes for the removal of natural organic matter. Water Res 45, 3263–3269. https://doi.org/10.1016/j.watres.2011.03.038.

Leresche, F., McKay, G., Kurtz, T., von Gunten, U., Canonica, S., Rosario-Ortiz, F.L., 2019. Effects of ozone on the photochemical and photophysical properties of

dissolved organic matter. Environ. Sci. Technol. 53, 5622–5632. https://doi.org/10.1021/acs.est.8b06410.
Lester, Y., Sharpless, C.M., Mamane, H., Linden, K.G., 2013. Production of photo-oxidants by dissolved organic matter during UV water treatment. Environ. Sci. Technol. 47, 11726–11733. https://doi.org/10.1021/es402879x.
Lundqvist, M.J., Eriksson, L.A., 2000. Hydroxyl radical reactions with phenol as a model for generation of biologically reactive tyrosyl radicals. J. Phys. Chem. B 104, 848–855. https://doi.org/10.1021/jp993011r.
McKay, G., Rosario-Ortiz, F.L., 2015. Temperature dependence of the photochemical formation of hydroxyl radical from dissolved organic matter. Environ. Sci. Technol. 49, 4147–4154. https://doi.org/10.1021/acs.est.5b00102.
Miller, W.L., Kester, D.R., 1988. Hydrogen peroxide measurement in seawater by (p-hydroxyphenyl) acetic acid dimerization. Anal. Chem. 60, 2711–2715. https://doi.org/10.1021/ac00175a014.
Mostafa, S., Rosario-Ortiz, F.L., 2013. Singlet oxygen formation from wastewater organic matter. Environ. Sci. Technol. 47, 8179–8186. https://doi.org/10.1021/es401814s.
Page, S.E., Arnold, W.A., McNeill, K., 2011. Assessing the contribution of free hydroxyl radical in organic matter-sensitized photohydroxylation reactions. Environ. Sci. Technol. 45, 2818–2825. https://doi.org/10.1021/es2000694.
Palma, D., Sleiman, M., Voldoire, O., et al., 2020. Study of the dissolved organic matter (DOM) of the Auzon cut-off meander (Allier River, France) by spectral and photoreactivity approaches. Environ Sci Pollut Res 27, 26385–26394. https://doi.org/10.1007/s11356-020-09005-7.
Patel-Sorrentino, N., Mounier, S., Lucas, Y., Benaim, J.Y., 2004. Effects of UV–visible irradiation on natural organic matter from the Amazon basin. Sci. Tot. Environ. 321, 231–239. https://doi.org/10.1016/j.scitotenv.2003.08.017.
Paul, A., Dziallas, C., Zwirnmann, E., Gjessing, E.T., Grossart, H.P., 2012. UV irradiation of natural organic matter (NOM): impact on organic carbon and bacteria. Aquat Sci 74, 443–454. https://doi.org/10.1007/s00027-011-0239-y.
Pearson, G.S., 1963. The photoxidation of acetone. J. Chem. Phys. 67, 1686–1692. https://doi.org/10.1021/j100802a026.
Polewski, K., Slawinska, D., Slawinski, J., Pawlak, A., 2005. The effect of UV and visible light radiation on natural humic acid and EPR spectral and kinetic studies. Geoderma 126, 291–299. https://doi.org/10.1016/j.geoderma.2004.10.001.
Rosario-Ortiz, F.L., Canonica, S., 2016. Probe compounds to assess the photochemical activity of dissolved organic matter. Environ Sci Technol 50, 12532–12547. https://doi.org/10.1021/acs.est.6b02776.
Sarathy, S.R., Stefan, M.I., Royce, A., Mohseni, M., 2011. Pilot-scale UV/H_2O_2 advanced oxidation process for surface water treatment and downstream biological treatment: effects on natural organic matter characteristics and DBP formation potential. Environ. Technol. 32, 1709–1718. https://doi.org/10.1080/09593330.2011.553843.
Sarathy, S.R., Mohseni, M., 2007. The Impact of UV/H_2O_2 advanced oxidation on molecular size distribution of chromophoric natural organic matter. Environ. Sci. Technol. 41, 8315–8320. https://doi.org/10.1021/es071602m.
Schmitt-Kopplin, P., Hertkorn, N., Schulten, H.R., Kettrup, A., 1998. Structural changes in a dissolved soil humic acid during photochemical degradation processes under O2 and N2 atmosphere. Environ. Sci. Technol. 32, 2531–2541. https://doi.org/10.1021/es970636z.
Sillanpää, M., ChakerNcibi, M., Matilainen, A., 2018. Advanced oxidation processes for the removal of natural organic matter from drinking water sources: a comprehensive review. J Environ. Manag. 208, 56–76. https://doi.org/10.1016/j.jenvman.2017.12.009.
Soman, A., Qiu, Y., Chan Li, Q., 2008. HPLC-UV method development and validation for the determination of low level formaldehyde in a drug substance. J. Chromatogr. Sci. 46, 461–465. DOI:0.1093/chromsci/46.6.461.
Stefan, M., Hoy, A., Bolton, J.R., 1996. Kinetics and mechanism of the degradation and mineralization of acetone in dilute aqueous solution sensitized by the UV photolysis of hydrogen peroxide. Environ. Sci. Technol. 30, 2382–2390. https://doi.org/10.1021/es950866i.
Stefan, M.I., Bolton, J.R., 1999. Reinvestigation of the acetone degradation mechanism in dilute aqueous solution by the UV/H_2O_2 Process. Environ. Sci. Technol. 33 (6), 870–873. https://doi.org/10.1021/es9808548.
Sun, L., Qian, J., Blough, N.V., Mopper, K., 2015. Insights into the photoproduction sites of hydroxyl radicals by dissolved organic matter in natural waters. Environ. Sci. Technol. Lett. 2 (12), 352–356. https://doi.org/10.1021/acs.estlett.5b00294.
Sun, Q., Ma, J., Yan, S., Song, W., 2021. Photochemical formation of methylhydroperoxide in dissolved organic matter solutions. Env. Sci. Technol. 52, 1076–1087. https://doi.org/10.1021/acs.est0c07717.
Tafer, R., Sleiman, M., Boulkamh, A., Richard, C., 2016. Photomineralization of aqueous salicylic acids. Photoproducts characterization and formation of light induced secondary OH precursors (LIS-OH). Water Res 106, 496–506. https://doi.org/10.1016/j.watres.2016.10.038.
Tang, W.W., Zeng, G.M., Gong, J.-.L., Liang, J., Xu, P., Zhang, C., Huang, B.-.B., 2014. Impact of humic/fulvic acid on the removal of heavy metals from aqueous solutions using nanomaterials: a review. Sci. Total Environ. 468–469, 1014–1027. https://doi.org/10.1016/j.scitotenv.2013.09.044.
Thomson, J., Roddick, F.A., Drikas, M., 2004. Vacuum ultraviolet irradiation for natural organic matter removal. J. Water Supply Res. Technol. - Aqua 53, 193–206. https://doi.org/10.2166/aqua.2004.0017.
Varanasi, L., Coscarelli, E., Khaksari, M., Mazzoleni, L.R., Minakata, D., 2018. Transformations of dissolved organic matter induced by UV photolysis, Hydroxyl radicals, chlorine radicals, and sulfate radicals in aqueous-phase UV-Based advanced oxidation processes. Water Res 135, 22–30. https://doi.org/10.1016/j.watres.2018.02.015.
Vaughan, P.P., Blough, N.V., 1998. Photochemical formation of hydroxyl radical by constituents of natural waters. Environ. Sci. Technol. 32, 2947–2953. https://doi.org/10.1021/es9710417.
Vidal, E., Negro, A., Cassano, A., Zalazar, C., 2015. Simplified reaction kinetics, models and experiments for glyphosate degradation in water by the UV/H2O2 process. Photochem. Photobiol. Sci. 14, 366–377. https://doi.org/10.1039/C4PP00248B.
Vione, D., Minella, M., Maurino, W., Minero, C., 2014. Indirect photochemistry in sunlit surface waters: photoinduced production of reactive transient species. Chem. Eur. J. 20, 10590–10606. https://doi.org/10.1002/chem.201400413.
Westerhoff, P., Mezyk, S.P., Cooper, W.J., Minakata, D., 2008. Electron Pulse Radiolysis Determination of Hydroxyl Radical Rate Constants with Suwannee River Fulvic Acid and Other Dissolved Organic Matter Isolates. Env. Sci Technol 41, 4640-4640. https://doi.org/10.1021/es062529n.
Wang, D., Duan, X., He, X., Dionysiou, D.D., 2016. Degradation of dibutyl phthalate (DBP) by UV-254nm/H2O2 photochemical oxidation: kinetics and influence of various process parameters. Environ. Sci. Pollut. Res. Int. 23, 23772–23780. https://doi.org/10.1007/s11356-016-7569-1.
Weisshar, J., Aiken, G.R., Bergamaschi, B.A., Fram, M.S., Fugii, R., Mopper, K., 2003. Evaluation of specific ultraviolet absorbance as an indicator of the chemical composition and reactivity of dissolved organic carbon. Environ. Sci. Technol. 37, 4702–4708. https://doi.org/10.1021/es030360x.
Wenk, J., Aeschbacher, M., Sander, M., von Gunten, U., Canonica, S., 2015. Photosensitizing and inhibitory effects of ozonated dissolved organic matter on triplet-induced contaminant transformation. Environ. Sci. Technol. 49, 8541–8549. https://doi.org/10.1021/acs.est.5b02221.
Yu, J., Flagan, R., Seinfeld, J., 1998. Identification of Products Containing -COOH, -OH, and –C=O in atmospheric oxidation of hydrocarbons. Environ. Sci. Technol. 32, 2357–2370. https://doi.org/10.1021/es980129x.
Yu, X.Y., Barker, J.R., 2003. Hydrogen peroxide photolysis in acidic aqueous solutions containing chloride ions. I. chemical mechanism. J. Phys. Chem. A 107 (9), 1313–1324. https://doi.org/10.1021/jp0266648.
Zhang, S., Rougé, V., Gutierrez, L., Croué, J.P., 2019. Reactivity of chromophoric dissolved organic matter (CDOM) to sulfate radicals: reaction kinetics and structural transformation. Water Res. 163, 114846 https://doi.org/10.1016/j.watres.2019.07.013.
Zhong, X., Cui, C., Yu, S., 2017. Identifying oxidation intermediates formed during ozone-UV of fulvic acid. Desalination Water Treat. 74, 258–268. https://doi.org/10.5004/dwt.2017.20587.
Zhou, Y., Cheng, F., He, D., Zhang, Y., Qua, J., Yang, X., Chenc, J., Peijnenburg, W.J.G.M., 2021. Effect of UV/chlorine treatment on photophysical and photochemical properties of dissolved organic matter. Water Res. 192, 116857 https://doi.org/10.1016/j.watres.2021.116857.
Zoschke, K., Dietrich, N., Bornick, H., Worch, E., 2012. UV-based advanced oxidation processes for the treatment of odour compounds: efficiency and by-product formation. Water Res 46, 5365–5373. https://doi.org/10.1016/j.watres.2012.07.012.